Well-log parameterized full waveform inversion 2: formulation of the two-parameter case

Ninoska Amundaray, Scott Keating, Matthew Eaid, and Kris Innanen

ABSTRACT

Addition of prior information in elastic full waveform inversion (EFWI) tends to aid faster and better model convergence by prioritizing relevant features of the medium where the simulated waveform is propagating. When this is employed as a parameterization, FWI formulations can be slightly simplified by reducing the number of terms used during the inversion. This idea was previously applied to an isotropic-elastic medium, which utilized the correlation between well-log data to aid the construction of a single parameter by fitting a trendline. While, models obtained using a version of the single log-guided parameterization have demonstrated encouraging results when little data variation exists. In this study, we advocate the inclusion of another parameter to this type of formulation, as way to (1) capture larger data variation and (2) expand the applicability of the formulation. To accomplish this, we propose a method that captures information from a direction omitted by the first parameter (or trendline), by combining spatial geometry with principal component analysis (PCA). Current results obtained using the updated log-guided parameterization demonstrate some positive remarks in terms of model convergence and measured parameter variation. But, to further exploit the addition of the second term in FWI applications, more understanding about parameter tuning must be carry out.

INTRODUCTION

Characterizations of an elastic medium usually requires the inclusion of two or more parameters relating the stress and strain components of the stiffness matrix. This poses several challenges in multiparameter simultaneous full waveform inversion (FWI), due to the intrinsic nonlinearity of the method. To bypass some of the latter, the addition of prior information in FWI formulations (e.g., penalty terms) plays a relevant role in real case applications. Furthermore, as demonstrated by Eaid et al. (2021), if analysis of prior data demonstrates a strong correlation between the elastic parameters used during the inversion (e.g., P-wave velocity or V_P, S-wave velocity or V_S, and density or ρ). There is a chance to further simplify FWI formulations by modeling a single parameter that encapsulates the relationship between the analyzed elastic terms, instead modeling two or more parameters simultaneously.

Although, the benefits of a single term parameterization can provide plausible inverted models and prevent non-physical combinations of inverted parameters (e.g., V_P values into ρ). Some aspects of the elastic theory might be slightly contradicted by this parameterization, since established formulations require a certain number of coefficients to characterize an elastic medium. Likewise, in cases where data variation is anticipated, even if it is a small amount, inversion of a single parameter will most likely exclude information that deviates from a given trend.

Though in several applications, values that divert from a general background trend might be regarded as an anomaly or noise. For cases that examine the effects of reservoir depletion and carbon capture and storage (CCS), we can expect relevant information associated with values that deviate. Hence, exclusion of this information in the single term log-guided parameterization can limit its uses, and its intrinsic benefits (e.g., cross-talk mitigation). To expand the applicability of the single term log-guided parameterization, we advocate for the addition of a secondary parameter to the existing formulation in this investigation.

Here, we proposed a method that aids capturing information from another direction omitted by a main trend in a second parameter, combining ideas of spatial geometry, coordinate system transformations and principal component analysis (PCA). After updating the log-guided parameterization, the proposed method is then applied in a time-lapse setting using models for various stages of carbon dioxide (CO_2) injection at the Carbon Management Canada Newell County Facility (CMC Newell County Facility). Lastly, results obtained using the updated parameterization are compared with inverted models determined by utilizing $V_P - V_S - \rho$ parameterization and the single term log-guided parameterization for the same stages of CO_2 injection (Amundaray et al., 2022).

METHOD

Proposed formulation for a two-parameter log-guided model parameterization

Our proposed second parameter in the log-guided parameterization (κ) was determined under the assumptions that the first inversion parameter (η) is defined on the tangent direction of the trendline. This can be defined using the arc length parameterization as proposed by Eaid et al. (2021). In a $V_P - V_S - \rho$ space, the arc length is expressed as

$$\eta_n = \eta_{n-1} + \sqrt{(\rho_n - \rho_{n-1})^2 + (V_{P_n} - V_{P_{n-1}})^2 + (V_{S_n} - V_{S_{n-1}})^2} \tag{1}$$

From the trendline, we expect that any other significant direction that captures any parameter variation will be found in a normal plane defined from the trendline itself. Equation 2 summarizes the expression for any given log value

$$\mathrm{P}_L = \hat{\eta} + a\hat{\kappa} \tag{2}$$

Where P_L is the well-log value, $\hat{\eta}$ is a reference point along the tangent direction, a is a scalar term that indicates a shift from the tangent, and $\hat{\kappa}$ is a fixed direction from the tangent.

The estimation κ was achieved combining concepts of spatial geometry, coordinate system transformations and PCA adapted to the defined trendline. For each sample along the trend, we propose:

1. Define a fixed vicinity of interest along the trendline.
2. Project every value that is within the established vicinity into a normal plane, which should be defined from the tangent plane.

3. Estimate the most significant direction from the trendline using PCA.

4. Use the estimated direction from step (4) to define κ.

To properly incorporate the second parameter in the inversion, FWI sensitivities must be updated based in η and κ, which leads to expressions of the form:

$$(\frac{\partial \rho}{\partial \eta} + \frac{\partial \rho}{\partial \kappa}) \tag{3}$$

$$(\frac{\partial c_{11}}{\partial \eta} + \frac{\partial c_{11}}{\partial \kappa}) \tag{4}$$

$$(\frac{\partial c_{44}}{\partial \eta} + \frac{\partial c_{44}}{\partial \kappa}) \tag{5}$$

With $c_{11} = V_P \rho$, $c_{44} = V_S \rho$, where V_P, V_S, and ρ are the P-wave velocity, S-wave velocity, and density terms from the trendline. Where terms $\partial\rho/\partial\eta$, $\partial c_{11}/\partial\eta$, $\partial c_{44}/\partial\eta$, $\partial\rho/\partial\kappa$, $\partial c_{11}/\partial\kappa$, $\partial c_{44}/\partial\kappa$ are the derivatives with respect to η and κ, which are numerically calculated using finite difference approximations. Lastly, Equation 2 is used to map model updates in η and κ back to $V_P - V_S - \rho$ space by updating c_{11}, c_{44} and ρ.

Modeled experiments

Three phases of CO_2 injection were modeled in this investigation using projections from the CMC Newell County Facility. These correspond to a stage prior to any gas injection, which we will refer as baseline, and two stages after 266 tons and 1664 tons of CO_2 are injected in the reservoir, which we will refer as medium and final stages. For these last two, it is assumed a horizontal migration of the CO_2 effects centered in an injection well at the reservoir level, which is identified between 295.65 m to 301.65 m (Macquet et al., 2019).

To generate the models used in the inversion, the well-log values were mapped from a $V_P - V_S - \rho$ space to η using the estimated trendline and Equation 1 following the steps described in Eaid et al. (2021). Likewise, we assume that all model contributions will be initially describe by the parameter along the tangent (i.e., η); hence, the second parameter was set to zero. Under this hypothesis, we expect that any relevant information that cannot be describe by η, will be added to κ as the inversion progresses. Figure 1 shows the true and initial models for V_P, V_S, ρ, η, and κ for reference.

As discussed in the previous section, a vicinity along the trendline must be established in order to estimate κ when using our proposed method. To accomplish this, we define a fixed cylinder. To assess the effects of the cylinder measurements, we tested three combinations of length and radius. While the cylinder length was set by trial and error as, 100 and 150. The radius was defined after plotting the well-log data, the trendline and a fixed deviation from the main trend, as shown in Figure 2. We decided to utilize 120 and 180 as cylinder radius during testing. When using the first, we are suggesting a small vicinity along the trend, where log values might be still relatively close to the trendline to estimate

κ. Whereas, when utilizing the second values will include log samples that might scattered further away from the trend.

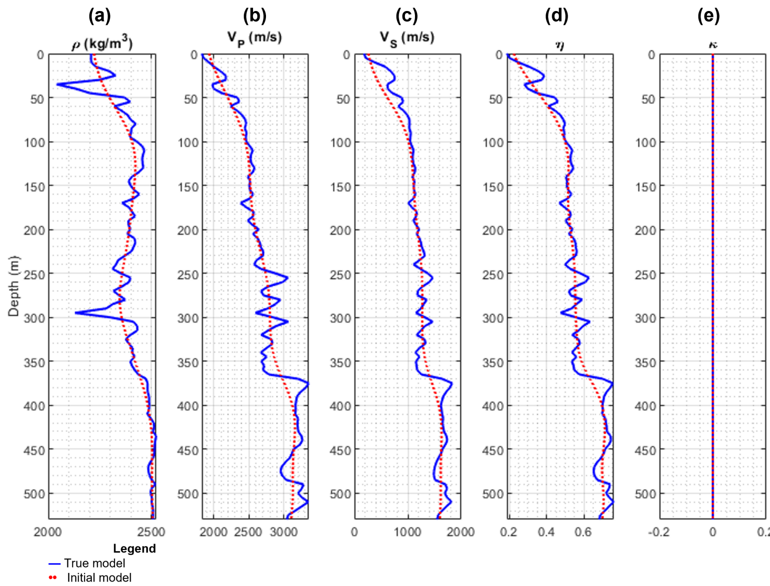

FIG. 1. Adapted well-logs and mapped parameters used during the inversion. In (a) density, (b) P-wave velocity, (c) S-wave velocity, (d) mapped η parameter, and (e) defined κ parameter. For each case, the blue lines represent the true model and the red dotted lines represent the initial models.

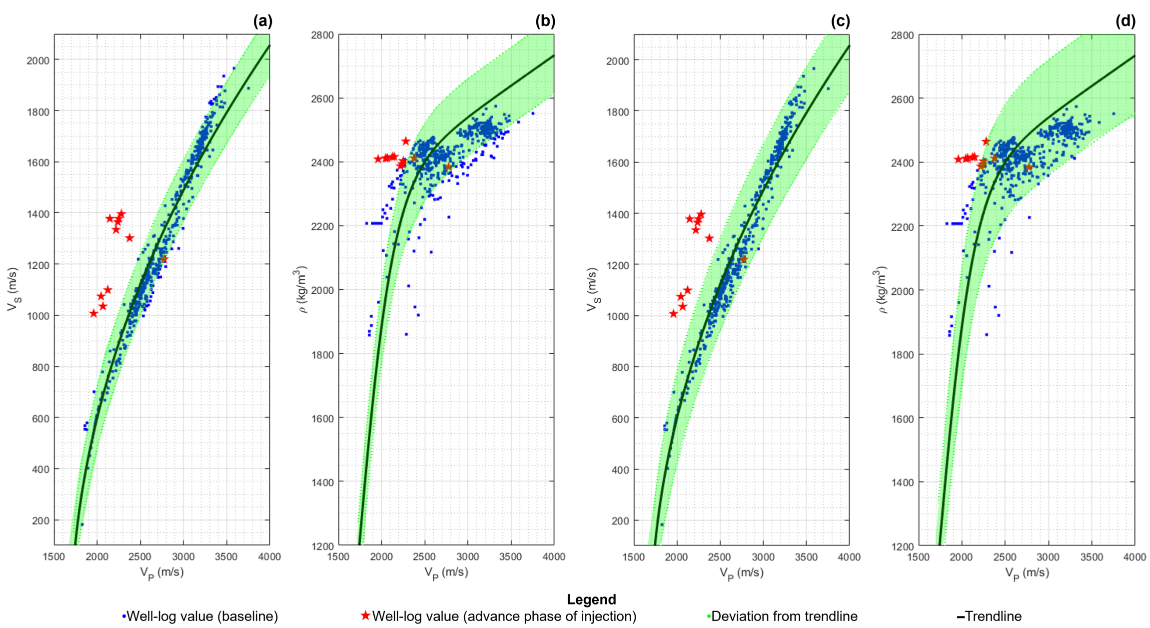

FIG. 2. Cross plots of V_S with respect to V_P, and ρ with respect to V_P given two constant deviations from the trendline. For (a) and (b) a deviation of 120 was defined from the main trend, and for (c) and (d) a deviation of 180 was defined. In every figure, the blue dots correspond to well-log values from a baseline stage, the red stars highlight the well-log values from an advanced stage of injection, the black line is the estimated trendline, and the green shaded area represents the edges of the vicinity considered during tests.

A fixed VSP configuration, similar to the permanent experiment deployed at the CMC Newell County Facility was used for modeling purposes in this investigation (Hall et al., 2018). As Figure 3(a) shows, receivers were set 20 m from the zero offset at the expected location of the observation well. While vertical receivers spanned every 5 m between 190 to 305 m. Modeled sources were located at the surface with a separation of 60 m each.

To maintain some level of consistency between the estimated models, we used the same number of frequency bands, iterations, and a similar weight for a regularization term during each modeled inversion. Though, the results using the well-log parameterization can be considered as a simultaneous inversion. Results using $V_P - V_S - \rho$ showed in this report cannot be regarded as a simultaneous case. These were obtained following a scaled approach as further explained in Amundaray et al. (2022), where V_P and V_S were simultaneously inverted and then, ρ was inverted separately, due to parameter cross-talk.

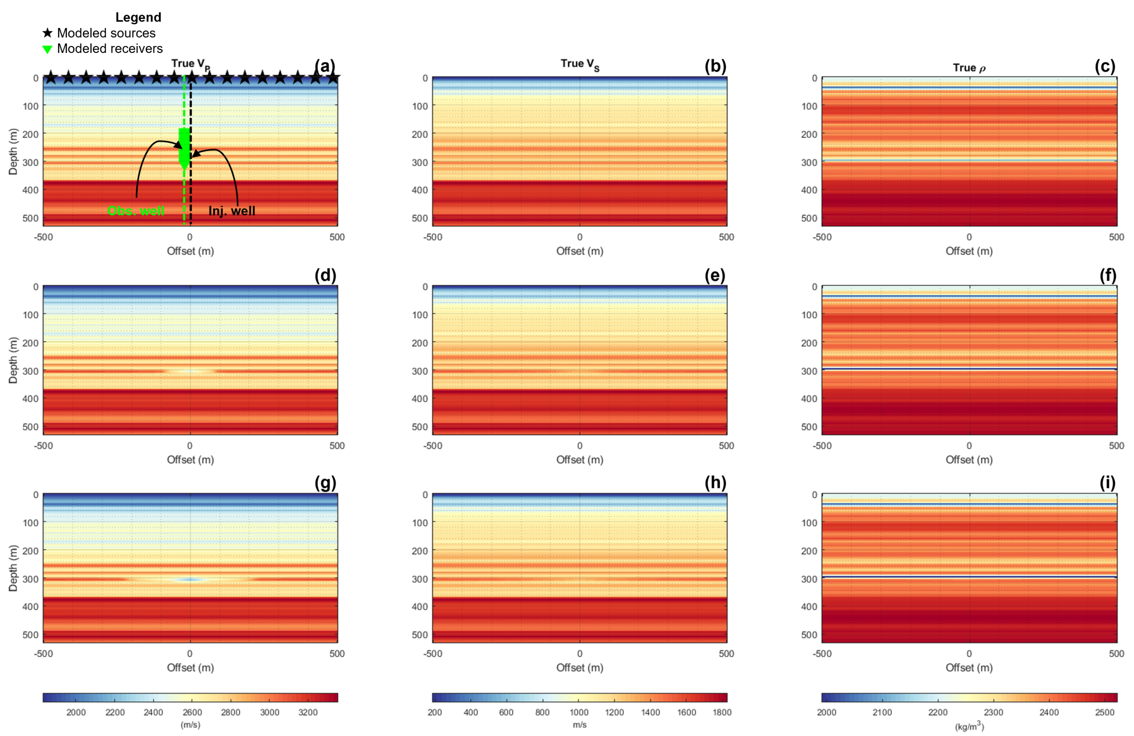

FIG. 3. True V_P, V_S, and ρ models corresponding to the three simulated stages. Models (a), (b), and (c) correspond to the baseline stage, models (d), (e), and (f) correspond to the medium injection stage, and models (g), (h), and (i) correspond to the final injection stage. Furthermore, an schematic of the seismic experiment and configuration of the CMC Newell County Facility is overlaid on (a). The black stars indicate the source locations, the green triangles indicate the receivers, the green dashed line indicates the observation well, and the black dashed line indicates the injection well.

RESULTS

Figure 4 shows V_P results using the two-parameter log-guided parameterization after η and κ were mapped back to $V_P - V_S - \rho$ space. These models were obtained using three different combinations of a fixed cylinder along the trendline to define a vicinity of interest and estimate κ. They correspond to a baseline stage, and as demonstrated, they reproduce the flat layer geometry expected at the CMC Newell County Facility. As observed in Figure 4 (a)-(c), increasing the length of the testing cylinder allows to image finer details of the overall velocity model, independently of the used radius size. Nonetheless, as shown in Figure 4 (d)-(e), at the profiles locations set at 20 m and 140 m from the zero offset (i.e., the injection well position), the effects of the used cylinder parameters appear to be minor.

The previous statement is partly supported by the calculated NRMSE at the defined offset locations, as summarized in Table 1. Though, overall values per modeled parameter are fairly similar, it appears that lower NRMSE were determined when using a combination of a large cylinder and large radius. Likewise, in general terms the NRMSE suggest better model convergence in these tests for V_P, followed by V_S, and lastly ρ.

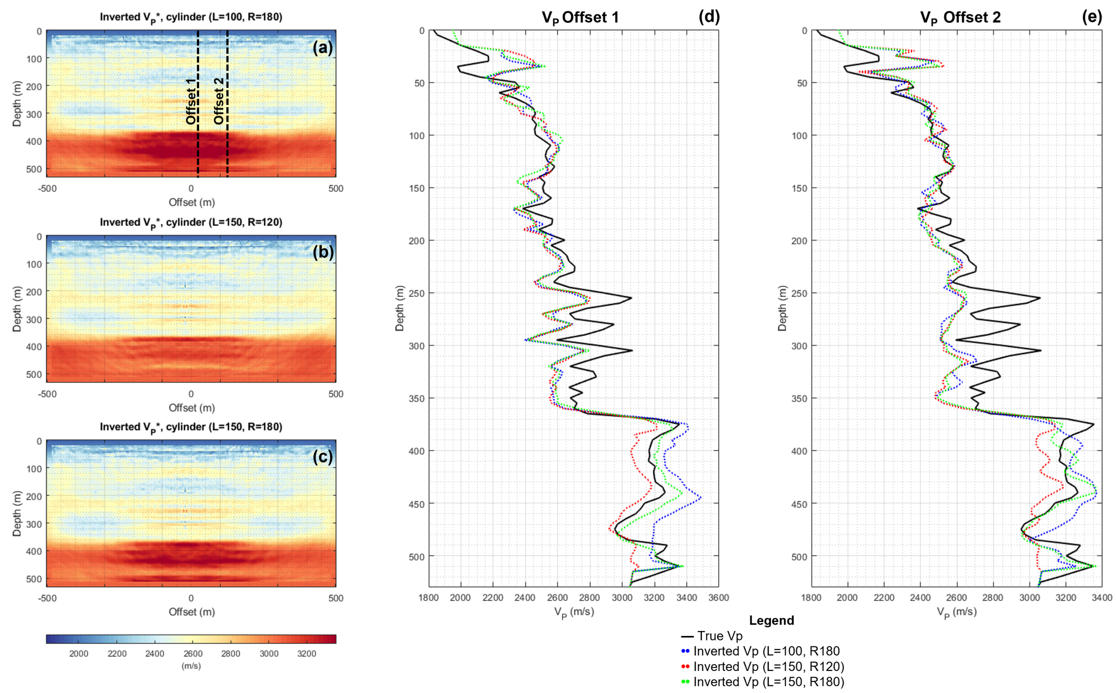

FIG. 4. Inverted V_P after η and κ were mapped back to $V_P - V_S - \rho$ space. Inverted models in (a), (b), and (c) were obtained varying the length (L) and radius (R) of a cylinder along the trendline to estimate κ. These three models correspond to the baseline stage. A profile view with examples of the inverted V_P values at two defined offsets are shown in (d) and (e). In the profile views, the black lines represent the true V_P, the blue dotted lines represent the inverted V_P using a cylinder with a length of 100 and a radius of 180, the red dotted lines represent the inverted V_P using a cylinder with a length of 150 and a radius of 120, and the green dotted lines represent the inverted V_P using a cylinder with a length of 150 and a radius of 180.

Table 1. Inverted ρ, V_P, and V_S from the baseline stage, in terms of the NRMSE at two offset locations using three cylinder combinations.

Cylinder dimension	Parameter	NRMSE	
		Offset 1	Offset 2
length = 100, radius = 180	ρ	0.2553	0.2299
	V_P	0.0972	0.1025
	V_S	0.687	0.0892
length = 150, radius = 120	ρ	0.2446	0.2537
	V_P	0.0919	0.1102
	V_S	0.0773	0.0982
length = 150, radius = 180	ρ	0.2448	0.2373
	V_P	0.0863	0.0997
	V_S	0.0714	0.0855

Figure 5 shows V_P, V_S, and ρ inverted models using the updated log-guided parameterization for the three stages of CO_2. A penalty term that encourages a flat-layer subsurface geometry was used for all cases with a similar weight. Although, we observed a good level of model convergence for both, V_P and V_S, including a continuous reduction of both velocities from baseline to an advanced injection stage. Density shows poor parameter imaging, which gets augmented with increasing offset.

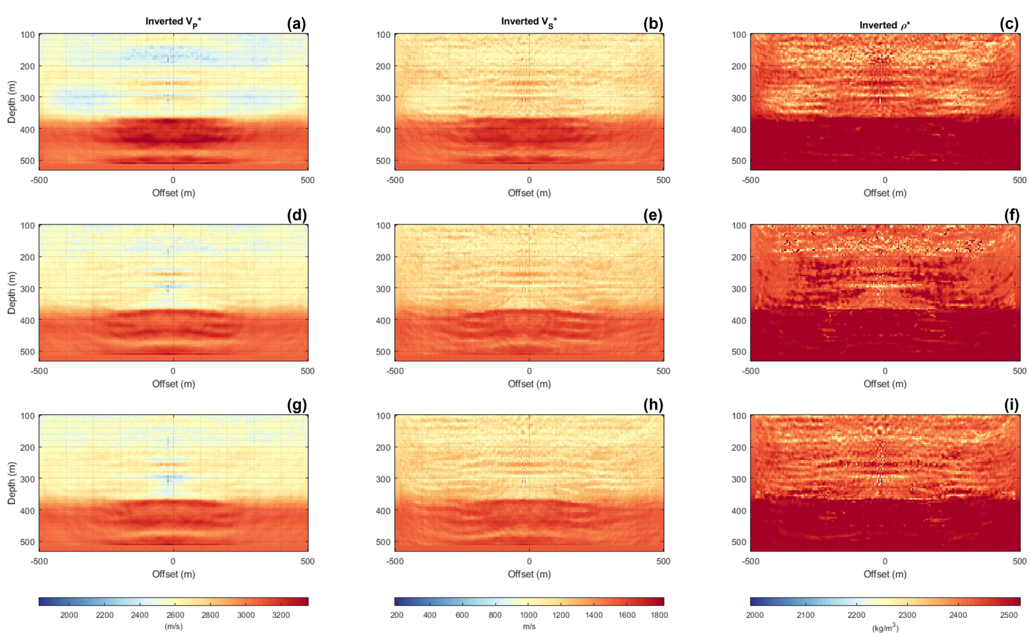

FIG. 5. Inverted models after η and κ were mapped back to $V_P - V_S - \rho$ space. Models (a), (b) and (c) correspond to the baseline stage, models (d), (e) and (f) corresponds to the medium injection stage, and models (g), (h) and (i) corresponds to the final injection stage.

Figure 6 shows a detailed view the from models shared in Figure 5 at an offset location set 20 m from the injection well location (i.e., zero offset). Here, it is noticeable that inverted V_P values appear to slightly underestimate the true log values between 250 m and 350 m. This a consistent behaviour for every modeled stage, as seen in Figure 6(a)-(c). Meanwhile for V_S, inverted models show a good level of agreement with the true model between 50 m to 350 m, as shown in Figure 6(d)-(f). But as already mentioned, density was poorly inverted at most depth levels. As shown in Figure 6(g)-(i), the majority of values are either underestimated or overestimated with respect to the true model.

Assuming a certain caveat, regarding the current level of certainty provided by the estimated models using our updated parameterization. We determined the model residuals that correspond to the medium and final phases of injection with respect to the inverted baseline. This was done to examine the extension of the CO_2 effects, and to compare the measured parameter variations at each stage.

Figure 7 and Figure 8 show the model residuals for V_P, V_S, and ρ. As expected from true models (see Figure 3), CO_2 effects are more distinguishable in the P-wave velocity parameter, in terms of the measured values and migration shape that radiates from the injection well. While, results with the two-parameter log guided-parameterization support the decrease of V_P for both, medium and final stages, the limits of the plume are surrounded by artifacts due to model residuals. This is more notorious in the final injection stage as illustrated in Figure 8.

As shown in Figure 7 and Figure 8, S-wave velocity residuals from the inverted model using the updated log-guided parameterization are severely surrounded by artifacts associated to the model residuals, which are non-related to the expected CO_2 effects. This makes interpretable results a little challenging at this moment. Nonetheless, it is worth mentioning that the latter was also observed in models residuals corresponding to other parameterizations, as mentioned in Amundaray et al. (2022).

Though, model residuals for V_P and V_S reproduce the expected limits of CO_2 effects in these elastic parameters. Results for ρ only reproduce a small decrease in this parameter, which produces a fainted shadow at the injection well location. Likewise, it is important to notice that the shape of the gas effects inverted in this study greatly differs with the proposed effects in the true model residuals, as seen in Figure 7(c) and Figure 8(c). This could be related to the use of log-guided parameterization, where parameters are coupled to each other and only a single combination of these is encouraged.

DISCUSSION

Synthetic models inverted for three stages of CO_2 injection at the CMC Newell County Facility using a two-parameter log-guided model parameterization suggest both, positive and challenging aspects of its use in a time-lapse setting. This is with respect to the estimated magnitude values for V_P, V_S, and ρ. Though more relevant, in regards to the capacity of clearly image the lateral extension of gas effects. While both, magnitude and geometry, associated to CO_2 changes are highly important in CCS applications. The latter is fundamental to ensure a secured containment of the gas in the subsurface.

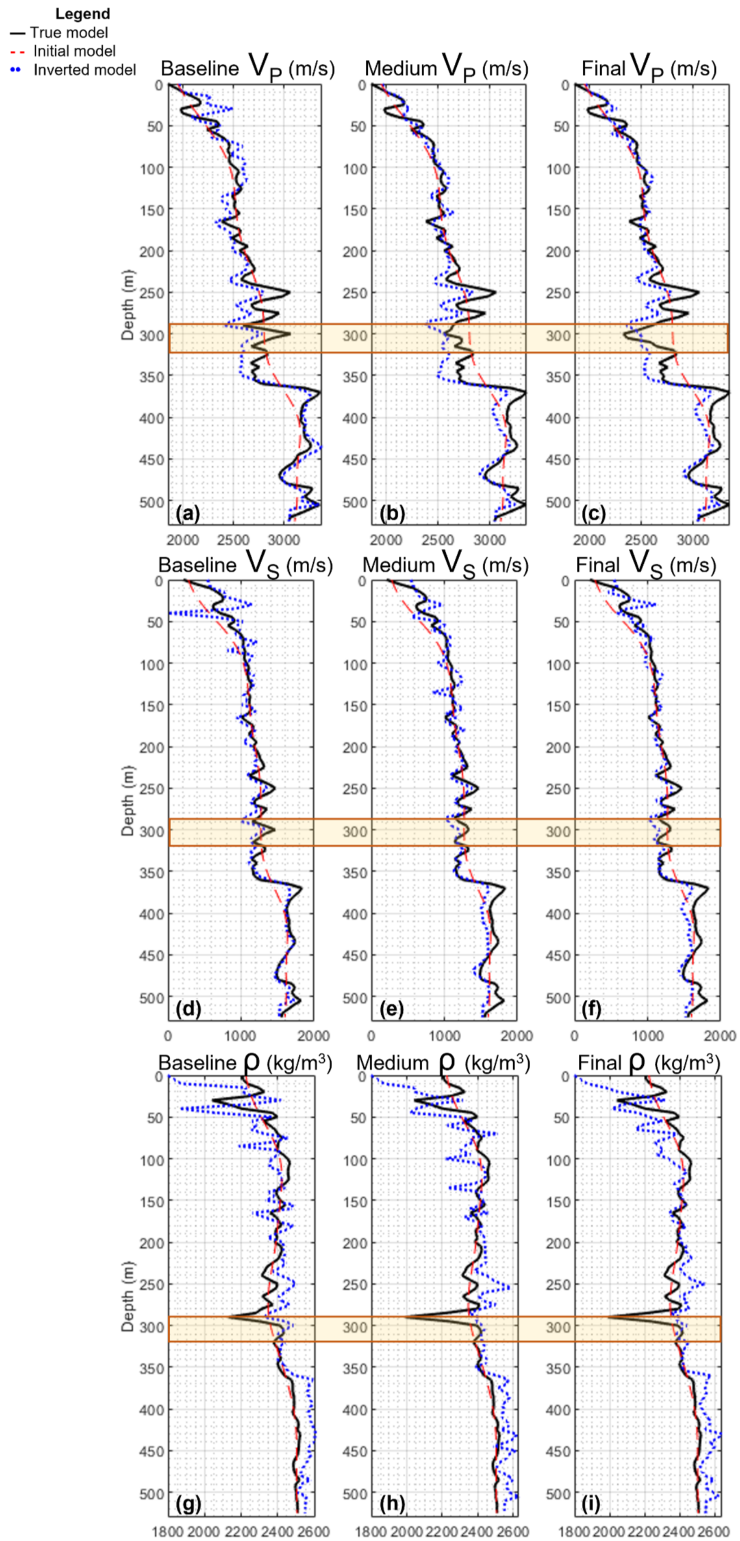

FIG. 6. Inverted V_P, V_S, and ρ using the two-parameter log-guided paramaterization at an offset location set 20 m from the zero offset. Profile views (a), (b), and (c) are associated to V_P, (d), (e), and (f) are associated to V_S, and (g), (h), and (i) are associated to ρ. For each, the black lines are the true models, the red dashed lines are the initial models, the blue dotted lines are the inverted models, and the yellow boxes indicate the reservoir level.

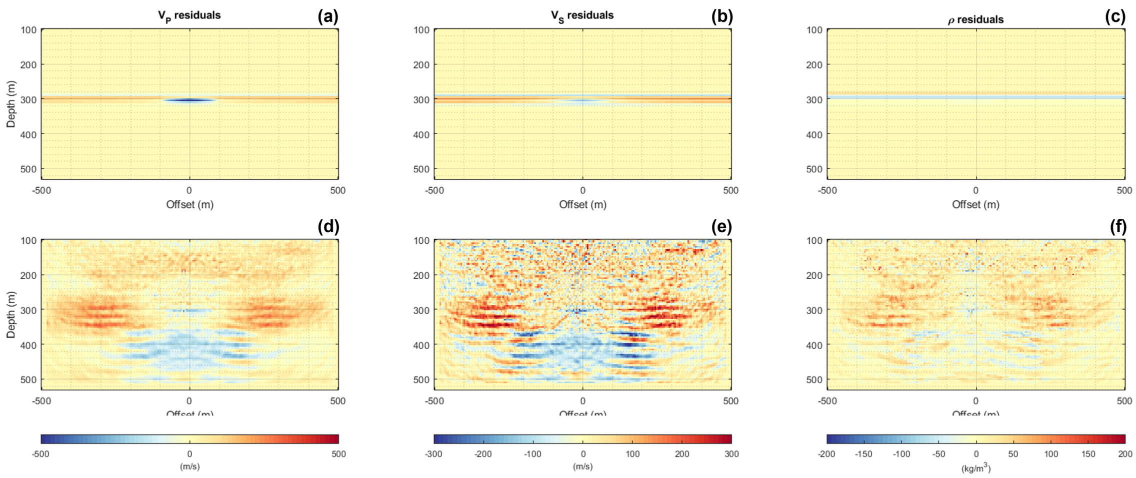

FIG. 7. Model residuals at a medium phase of injection taking as reference the inverted baseline. Models in (a), (b) and (c) are the true model residuals, and (d), (e) and (f) are residuals from the inverted models.

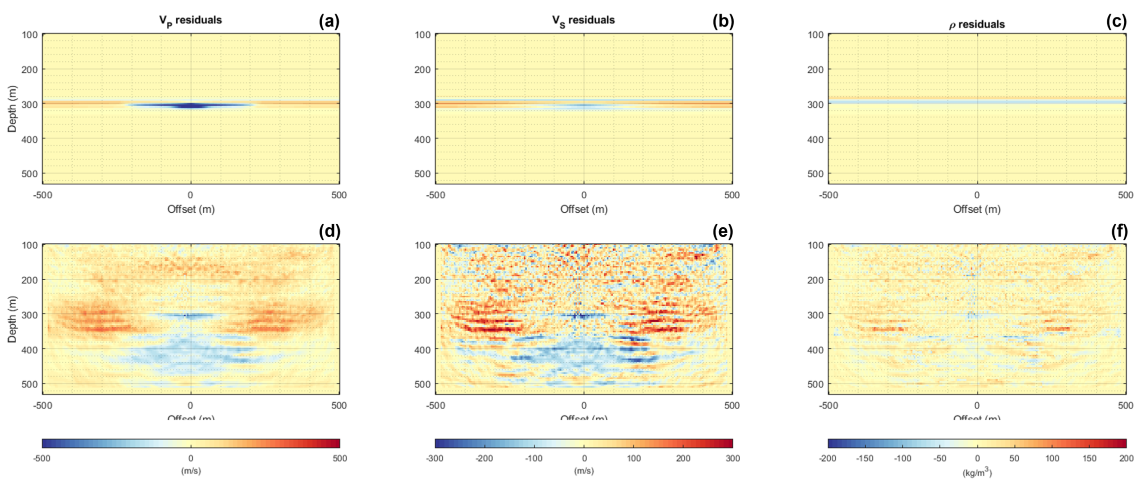

FIG. 8. Model residuals at the final phase of injection taking as reference the inverted baseline. Models in (a), (b) and (c) are the true model residuals, and (d), (e) and (f) are residuals from the inverted models.

Our current results demonstrate a good level of model convergence with respect to the true models, which is better observed in V_P, followed by V_S and then, ρ. For each, the inverted models that were mapped from our two defined terms η and κ in the log-guided parameterization, exhibit a continuous magnitude decrease at the reservoir level. These values are similar to those suggested by the true models and model residuals, as shown in Figure 6. Though, the inverted models in this study underestimate some features from the true models. They represent a relative improvement from results using a single parameter log-guided paramereterization for the same simulated stages. For this, inverted models show larger parameter over-and-underestimation (Amundaray et al., 2022), as also suggested by the calculated NRMSE values shown in Table 2. This remark is encouraging because it suggest that the updated formulation can reproduce interpretable models with additional details that are captured in the model by the inclusion of the second parameter.

A relevant drawback in our current inverted models is associated with modeling artifacts that appear in some of our inverted baseline models. These generally emerge with increasing offset, surrounding the reservoir level and eventually limiting of imaging the lateral effects of the CO_2 when using them as reference to generate model residuals. Nonetheless, as shown in Figure 5, CO_2 changes are still observable in the inverted models, especially near the zero offset. Yet, again the lateral extension are poorly distinguished with increasing offset.

Table 2. Comparison of inverted models using three parameterizations in terms of the NRMSE.

Modeled stage	Parameter	NRMSE		
		Parameterization		
		$V_P - V_S - \rho$	Single log	Two-parameter log
Baseline	ρ	0.1729	0.2228	0.1879
	V_P	0.1012	0.1473	0.1519
	V_S	0.1057	0.1285	0.1336
Medium	ρ	0.1294	0.1905	0.1689
	V_P	0.1046	0.1475	0.1333
	V_S	0.1091	0.1318	0.1288
Final	ρ	0.1379	0.1867	0.1539
	V_P	0.1027	0.1423	0.1293
	V_S	0.1107	0.1296	0.1307

CONCLUSIONS

Inverted models using our suggested update to the log-guide parameterization by incorporating a second parameter is currently reproducing interpretable results. Though, inverted values partly converged towards the true solution, they show parameter underestimation and overestimation at the reservoir level. This can be associated with a poorly fine-tuning process of our second parameter or an intrinsic result of using a parameterization that bounds together V_P, V_S, and ρ. Nonetheless, as suggested by the NRMSE values the addition a second parameter aids the inversion of more accurate models, if it is compared with the single parameter log-guided parameterization results. This is more noticeable for density and P-wave velocity, but it is not always true for S-wave velocity. For the latter, inverted results using the single parameter reaches lower values of model misfit in some modeled stages when using the single parameter. While current results using either log-guide formulations do not reproduce models that demonstrate lower model misfit with respect to results using $V_P - V_S - \rho$ as parameterization (as suggested by the NRMSE). These formulations overcome the latter in terms of amount of time required by the inversion. Current application at the CMC Newell County Facility, using synthetic results require an scaled approach when using $V_P - V_S - \rho$ to obtain interpretable results, which is not required when applying the log-guided parameterization. Likewise, we must highlight that our inverted results using the log-guider parameterization capture both, the expected effects of parameter diminish and the lateral extend of these by the inclusion of CO_2 at the resevoir in the study site, which is an encouraging remark. Hence, we plan to further examine this formulation by fine-tuning the inversion parameters and potentially test it in other case scenarios.

ACKNOWLEDGEMENTS

We thank the sponsors of CREWES for continued support. This work was funded by CREWES industrial sponsors and NSERC (Natural Science and Engineering Research Council of Canada) through the grant CRDPJ 543578-19. We also acknowledge the Carbon Management Canada Newell County Facility for providing critical information for this investigation. Likewise, we thank Qi Hu for sharing his estimated well-logs for the study site.

REFERENCES

Amundaray, N., Keating, S., Eaid, M., and Innanen, K. A., 2022, Well-log parameterized full waveform inversion 1: analysis of the single parameter case: CREWES Research Report, **this volume**, No. 1.

Eaid, M., Keating, S., and Innanen, K. A., 2021, Full waveform inversion of DAS field data from the 2018 CaMI VSP survey: CREWES Research Report, **33**, No. 7.

Hall, K. W., Bertram, K. L., Bertram, M. B., Innanen, K. A. H., and Lawton, D. C., 2018, CREWES 2018 multi-azimuth walk-away VSP field experiment: CREWES Research Report, **30**, No. 16.

Macquet, M., Lawton, D. C., Saeedfar, A., and Osadetz, K. G., 2019, A feasibility study for detection for detections thresholds of co2 at shallow depths at the cami field research station, newell county, alberta, canada: Petroleum Geoscience, **25**, No. 4, 509–518.